The Effect of Single Atom Replacement on Organic Thin Film Transistors: Case of Thieno[3,2-b]pyrrole vs. Furo[3,2-b]pyrrole

Journal Name

ARTICLE

The Effect of Single Atom Replacement on Organic Thin Film Transistors: Case of Thieno[3,2-*b*]pyrrole vs Furo[3,2-*b*]pyrrole

Chandima Bulumulla,[a] Ruwan Gunawardhana,[a] Sang Ha Yoo,[c] Cody R. Mills,[a] Ruvanthi N. Kularatne,[a] Thomas N. Jackson,[d] Michael C. Biewer,[a] Enrique D. Gomez,[c,e] and Mihaela C. Stefan [a,b]

Despite polypyrrole having higher conductivities compared to polythiophenes, pyrrole based materials have garnered less attention in the organic electronics community due to their instability in air. Construction of stable pyrrolic units could be achieved by fusing relatively unstable pyrrole with stable aromatic rings. In this report, we discuss and compare the organic field-effect transistor performances of the smallest S,N-heteroacene and O,N-heteroacene; thieno[3,2-*b*]pyrrole and furo[3,2-*b*]pyrrole, respectively, in donor-acceptor-donor type organic semiconducting small molecules. Since both building blocks are highly electron-rich, thiophene flanked 5,6-difluorobenzo[*c*][1,2,5]thiadiazole is employed as a central electron-withdrawing unit. The small molecule containing thieno[3,2-*b*]pyrrole exhibit moderate hole mobilities (10^{-3} cm^2 /V s) irrespective of the annealing temperature. In contrast, the small molecule bearing furo[3,2-*b*]pyrrole is completely inactive in field-effect transistors. To the best of our knowledge this is the first report to compare the smallest units of S,N and O,N-heteroacenes for organic field-effect transistors.

Introduction

Over the last few years, a tremendous amount of research has been carried out in the area of organic field-effect transistors (OFETs), leading to high charge carrier mobilities up to 10 cm^2 /V s.[1-3] However, practical OFET applications require more than high charge carrier mobilities. It is perhaps equally important to achieve low threshold voltages, low subthreshold swings, and high on-to-off current ratios (I_{on}/I_{off}) for fast switching processes that can be triggered at low voltages.[4, 5] In order to fabricate reliable and reproducible OFETs, structural components, and self-assembly or molecular ordering should be precise.[6, 7] Although polymeric materials exhibit promising results, they suffer from irreproducible molecular weights and uncontrollable molecular weight distributions which lead to more batch-to-batch variations.[8-11] Therefore, organic semiconducting small molecules or oligomers with precise molecular weights have received significant attention.[12-15] Out of the many classes of semiconducting small molecules, linear acenes have been of great interest due to their high charge carrier mobilities and feasibility of control over fabrication.[16-21] Anthracene, the smallest building block in the class of acenes, have shown a hole mobility of 0.02 cm^2 /V s in single crystal thin film transistors.[22] By extending the conjugation using one more benzene ring, mobility was increased to 0.4 - 2.4 cm^2 /V s for tetracene.[23] Upon increasing conjugation length further with pentacene, a record high mobility of 5-40 cm^2 /V s was achieved in single crystal OFETs.[24, 25] It has been demonstrated and postulated that even higher performances could be attained for unsubstituted higher acenes, unfortunately, instability at ambient conditions and synthetic challenges limit these materials.[26-29] Furthermore, even though unsubstituted acenes appear promising from a performance perspective, from an economical perspective these materials do not add significant advantages compared to conventional silicon technologies since they require high temperature and vacuum processing conditions for fabrication. Therefore, in recent years, the field has focused on non-conventional materials that could mimic properties of acenes with the added advantage of solution processability. Oligothioacenes have been synthesized to lower the aromaticity, but charge carrier mobilities are somewhat lower compared to fused benzene rings.[30-33] Another interesting class of substituted acenes is heteroacenes.

Heteroacenes are prepared by introducing heteroatoms into the acene skeleton such as chalcogenides and nitrogen. The replacement of heteroatom influences both the electronic structure and crystal packing which eventually affects charge transport.[34] Unfortunately, the choice of heteroatom and impact on charge transport has been found to be complex. In the case of chalcogen based acenes, for dinaphthochalcogen-phenochalcogenophenes,[33] circulenes,[35, 36] and diphenylbenzodichalcogenophenes,[37] selenium was found to perform similar or better than sulfur, but the trend discontinues with tellurium. However, due to environmental toxicity caused by selenium and tellurium, interest in materials with either selenium or tellurium is limited. Since nitrogen has a

[a]The Department of Chemistry & Biochemistry and [b]Department of Bioengineering, The University of Texas at Dallas, Richardson, TX, 75080, United States
[c]The Department of Chemical Engineering, [d]Department of Electrical Engineering, and [e]Materials Research Institute, The Pennsylvania State University, University Park, PA 16802, United States
*Email - mci071000@utdallas.edu

comparable or smaller atomic radius as compared to carbon, and provide a synthetic site amenable for N-alkylation reactions to control the solubility, solution processable acene derivatives could be made easily.[38-41] To tune frontier energy levels and improve intramolecular charge transfer, thiophene-pyrrole based S,N-heteroacenes were introduced as non-conventional building blocks.[42-44] Unfortunately, these material have not been tested in electronic devices to evaluate their electrical performance. Instead of exploring higher linear S,N-heteroacenes, it is fundamentally important to understand the characteristics by first analyzing the smallest entity of the class. The smallest S,N-heteroacene; thieno[3,2-*b*]pyrrole have shown promising results in OFETs with linear transfer characteristics.[45] Recently, in our group, we showed that devices constructed from both small molecules and polymers of thieno[3,2-*b*]pyrrole could lead to high hole mobilities without sacrificing linear transfer characteristics.[46, 47] For our small molecule work, the choice of acceptor was thiophene and furan flanked benzo[*c*][1,2,5]thiadiazole units. Since the furan flanking unit leads to higher degree of backbone curvature and poor OFET performances, we have decided to employ thiophene flanked 5,6-difluorobenzo[*c*][1,2,5]thiadiazole to further increase the electron withdrawing nature of the acceptor. In recent reports, it has been shown that having fluorine atoms is beneficial for OFETs creating closer packing between electron-rich domains and electron-poor domains to reduce the energetic barrier for charge hopping.[48, 49] On the other hand, some reports claim fluorination is detrimental to OFETs, but it gives higher air stability due to the lowering of the HOMO level.[50, 51] Although these studies were conducted for polymeric materials, small molecular semiconductor materials have not been used to test the effect of fluorination for OFETs. To further expand the scope of our studies, we selected the smallest O,N-heteroacene, furo[3,2-*b*]pyrrole to examine the effect of the building block toward OFET properties. To the best of our knowledge, this is the first report of comparing an S,N-heteroacene vs O,N-heteroacene, and utilization of furo[3,2-*b*]pyrrole for OFETs. Fig 1 depict our work in context of previous efforts.
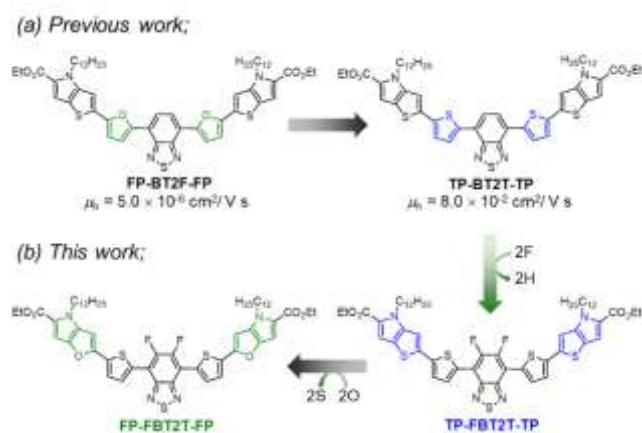

Fig 1 (a) Previous work based on thieno[3,2-b]pyrrole-benzothiadiazole based small molecules.[46] (b) The extension of the work through fluorination of benzothiadiazole and introduction of furo[3,2-*b*]pyrrole

Experimental

General measurements and characterization

All the intermediate and target compounds were characterized by ^{1}H NMR and ^{13}C NMR spectroscopy recorded on a 500 MHz Bruker AVANCE spectrometer using CDCl$_3$ as the solvent referenced at 7.26 ppm. Final semiconductors were further analyzed by MALDI-TOF spectroscopy to assess the molecular weight and purity. A Shimadzu Biotech Axima Confidence spectrometer was used in reflectron_HiRes mode with 2,2′:5′,2′′-terthiophene as the matrix in a matrix/analyte configuration. The UV-vis absorption profiles were measured with an Agilent 8453 UV-vis spectrophotometer. Dilute chloroform solutions of **TP-FBT2T-TP** and **FP-FBT2T-FP** were used for solution spectra while thin films made by drop-casting chloroform solutions on glass slides were used for thin film spectra. Cyclic voltammetry experiments were recorded on a BAS CV-50W voltammetry analyzer using three electrode system; a Pt inert working electrode, Pt wire auxiliary electrode and Ag/Ag$^+$ reference electrode. The redox potential of ferrocene/ferrocenium (F$_c$/F$_c^+$) was used to calibrate. A 0.1 M tetrabutylammonium hexafluorophosphate in anhydrous acetonitrile was used as the electrolyte under an argon atmosphere. The HOMO and LUMO energy levels were calculated from the following equations (1) and (2):

$$E_{HOMO} = -(\varphi_{ox} - \varphi_{Fc/Fc^+} + 4.8) \text{ eV} \qquad (1)$$

$$E_{LUMO} = -(\varphi_{red} - \varphi_{Fc/Fc^+} + 4.8) \text{ eV} \qquad (2)$$

Grazing-incidence wide-angle X-ray scattering (GIWAXS) measurements

GIWAXS experiments were carried out at beamline 11.3 of the Stanford Synchrotron Radiation Light source at the SLAC National Accelerator Laboratory. Data were collected using 12.7 keV X-rays and a Raxyonics 225 detector. The sample to beam distance was 315 mm, and an incidence angle of 0.10° was used to maximize scattering intensities. 2-D images were averaged in the out-of-plane (vertical) or in-plane (horizontal) direction to produce 1-D profiles as a function of scattering vector $q = 4\pi \text{Sin}(\theta/2)/\lambda$, where θ is the scattering angle and λ is the X-ray wavelength. The regions corresponding to the beam stop and scattering from the silicon substrate were omitted, such that 1-D scattering profiles have a q-range between 0.1 and 2.2 Å^{-1}. Thin films were prepared similarly to that of device fabrication to obtain a meaningful comparison.

Tapping mode atomic force microscopy (TMAFM) measurements

TMAFM images were recorded in between channel region using a Nanoscope IV Multimode Veeco instrument equipped with a vertical engage scanner. The TMAFM images were acquired using a Si cantilever with the resonance frequency of 320 kHz and spring constant of 42 N/m. AFM images with 2 × 2 μm scan size were recorded with a frequency of 1 Hz.

Fabrication and characterization of OFET devices

OFETs with common bottom-gate/bottom-contact configuration were employed to perform electrical characterizations. A highly doped n-type silicon wafer was used as the substrate with 200 nm thick thermally grown SiO_2 as the dielectric layer. First, Si/SiO$_2$ surface was covered with 5 nm chromium and 100 nm gold in-situ by Temescal E-beam evaporator. Cr/Au source and drain contacts were patterned using standard photolithographic techniques having different channel lengths and widths. After applying the photoresist on the electrodes, back of the silicon wafer was etched with 7:1 BOE solution from JT Baker and the gate electrode was created by deposition of 100 nm gold by an E-beam evaporator. OFET substrates were sonicated for 5 mins each time using semiconducting grade acetone, toluene, and 2-propanol. The capacitance per unit area was measured to be 17 nF cm^{-2}. The substrates were then cleaned by immersing in piranha solution (7:3 mixture of conc. sulfuric acid and 30% hydrogen peroxide) for 10 mins followed by rinsing with DI water and dried with nitrogen. An additional UV-ozone treatment was performed for 10 mins followed by washing again with DI water and dried with nitrogen. A self-assembled monolayer (SAM) of octadecylsilane (OTS) was prepared by the base (NH$_4$OH) vapor-catalyzed hydrolysis of octadecyltrimethoxysilane (OTMS) similar to previous reports.[46, 47] Briefly, 3 mM OTMS solution in trichloroethylene was added to cover the entire surface of Si/SiO$_2$ surface and allowed to partially assemble for 10 s and spun at 3000 rpm for 10 s. The base-catalyzed hydrolysis was performed by placing the substrates containing thin films inside a closed container with 3 mL of NH$_4$OH (28-30% NH$_3$ assay) in a vial for 10 h at room temperature. Substrates were rinsed with DI water and sonicated for 10 mins in toluene and dried by nitrogen. Small molecules **TP-FBT2T-TP** and **FP-FBT2T-FP** were dissolved in chloroform at a concentration of 5 mg/mL and 10 mg/mL, respectively. A thin layer was deposited by spin coating at 750 rpm for 30 s after covering the device surface for 30 s and 60 s with 70 µL of **TP-FBT2T-TP** and **FP-FBT2T-FP**, respectively. After annealing at different temperatures for 5 mins inside a nitrogen-filled glovebox, electrical measurements were performed in air at room temperature using Cascade Microtech Model Summit Microchamber with a Keithley 4200-SCS system.

Materials and synthetic details

Commercially available 2-thiophenecarboxyaldehyde 98% (Sigma Aldrich), furfural (Fischer Scientific, Reagent Grade), ethyl trifluoroacetate 99% (Alfa Aesar), 18-crown-6 ether $\geq$ 99% (Sigma Aldrich), 1-bromododecane 98% (Alfa Aesar) methoxy(cyclooctadiene)iridium(I) dimer (Ir[(μ_2-OMe)(COD)]$_2$), Ir nominally 58% (Alfa Aesar), 4,4'-di-*tert*-butyl-2,2'-dipyridyl (dtbpy, Sigma Aldrich), Pinacolborane 97% (HBpin, Acros Organics), tetrakis(triphenylphosphine)palladium(0) 99% (Sigma Aldrich), 1,4-dioxane (Fischer Scientific, Reagent Grade), octadecyltrimethoxysilane 90% (Acros Organics), hydrogen peroxide 30% (Acros Organics), ammonium hydroxide 28-30% (Merck) were used without further purification. Tetrahydrofuran and toluene were freshly distilled from a sodium-benzophenone ketyl prior to use.

Synthesis of ethyl-2-azido-3-(thiophen-2-yl)acrylate

To a 250 mL three-neck round bottomed flask was added sodium ethoxide (3.64 g, 53.5 mmol) with 48 mL of dry ethanol under nitrogen and cooled to 0 °C. In a separate vial 2-thiophenecarbaldehyde (3.00 g, 26.8 mmol), ethyl azidoacetate (6.90 g, 53.50 mmol), and ethyl trifluoroacetate (7.52 g, 53.3 mmol) were dissolved in 10 mL of dry ethanol. The mixture was added to the sodium ethoxide solution and stirred for 6 h at 0 °C. The reaction mixture was added to a saturated solution of ammonium chloride and extracted with diethyl ether (3 × 50 mL). The combined organic extracts were washed with DI water, brine, and concentrated under vacuo to give a crude residue. Pure compound was obtained as a yellow solid after purifying on column chromatography by using hexane: ethyl acetate (9:1 v/v) as the eluent. (5.50 g, Yield = 92%). ^{1}H NMR (CDCl$_3$, 500 MHz): δ_H 1.39 (t, 7.0 Hz, 3H), 4.36 (q, 7.0 Hz, 2H) 7.07 (dd, 3.5 Hz and 3.0 Hz, 1H), 7.17 (s, 1H), 7.32 (d, 3.5 Hz, 1H), 7.50 (d, 5Hz, 1H). ^{13}C NMR (CDCl$_3$, 125 MHz); δ_C 14.39, 62.28, 119.41, 122.86, 127.19, 130.54, 132. 11, 136.77, 163.34

Synthesis of ethyl-2-azido-3-(furan-2-yl)acrylate

Sodium ethoxide (3.64 g, 53.5 mmol) and 48 mL of dry ethanol were added to a 250 mL three-neck round bottomed flask under nitrogen and cooled to 0 °C. In a vial, furfural (3.00 g, 31.2 mmol), ethyl azidoacetate (7.69 g, 62.5 mmol), and ethyl trifluoroacetate (8.82 g, 62.5 mmol) were dissolved with 10 mL of dry ethanol. The mixture was added to the sodium ethoxide solution and stirred for 6 h at 0 °C. The brown solid obtained after quenching the reaction with saturated ammonium chloride was filtered and dried in air to afford the pure compound. (5.89 g, Yield = 91%). ^{1}H NMR (CDCl$_3$, 500 MHz): δ_H 1.37 (t, 7.5 Hz, 3H), 4.35 (q, 7.0 Hz, 2H), 6.52 (dd, 1.5 Hz and 2.5 Hz, 1H), 6.87 (s, 1H), 7.10 (d, 3.5 Hz, 1H), 7.49 (d, 3.5Hz, 1H). ^{13}C NMR (CDCl$_3$, 125 MHz); δ_C 14.35, 62.32, 112.73, 113.58, 115.32, 144.01, 149.69, 163.32

Synthesis of ethyl 4*H*-thieno[3,2-*b*]pyrrole-5-carboxylate

To 100 mL of toluene, ethyl-2-azido-3-(thiophen-2-yl)acrylate (3.60 g, 16.1 mmol) was added in portions and refluxed for 4 h. The resulting solution was cooled to room temperature and the solvent was removed under reduced pressure to obtain the pure compound. (2.67 g, Yield = 85%). ^{1}H NMR (CDCl$_3$, 500 MHz): δ_H 1.39 (t, 7.0 Hz, 3H) 4.36 (q, 7.0 Hz, 2H), 6.95 (d, 5.0 Hz, 1H), 7.14 (s, 1H), 7.33 (d, 5 Hz, 1H), 9.11 (s, 1H). ^{13}C NMR (CDCl$_3$, 125 MHz); δ_C 14.60, 60.81, 107.68, 111.19, 124.96, 127.24, 129.57, 141.33, 161.75

Synthesis of ethyl 4*H*-furo[3,2-*b*]pyrrole-5-carboxylate

To 100 mL of toluene, ethyl-2-azido-3-(furan-2-yl)acrylate (3.32 g, 16.1 mmol) was added and refluxed for 4 h. The resulting solution was cooled and toluene was removed in vacuo to obtain the pure compound. (2.76 g, Yield = 96%). ^{1}H NMR (CDCl$_3$, 500 MHz): 1.37 (t, 7.0 Hz, 3H) 4.35 (q, 7.0 Hz, 2H), 6.45 (d, 1.5 Hz, 1H), 6.80 (s, 1H), 7.51 (d, 2.0 Hz, 1H), 8.86 (s, 1H). ^{13}C NMR (CDCl$_3$, 125 MHz); δ_C 14.61, 60.63, 96.97, 99.04, 124.39, 128.78, 148.16, 148.72, 162.28

Synthesis of ethyl 4-dodecyl-4*H*-thieno[3,2-*b*]pyrrole-5-carboxylate

To a 100 mL three neck round bottomed flask, ethyl 4*H*-thieno[3,2-*b*]pyrrole-5-carboxylate (2.00 g, 10.3 mmol),

anhydrous potassium carbonate (2.83 g, 21.5 mmol), 18-crown-6 ether (catalytic amount) and dry *N,N*-dimethylformamide (36.0 mL) were added under nitrogen. Solution was stirred at 100 °C for 2 h before adding 1-bromododecane (5.28 g, 21.5 mmol). Resulting solution was refluxed for 12 h and cooled to room temperature. DI water (50 mL) was added and organic layer was extracted with ethyl acetate (3 × 30 mL). The organic layer was washed with brine, dried over anhydrous magnesium sulfate and concentrated. The crude was purified by column chromatography using hexane: ethyl acetate (99:1 v/v) as the eluent to obtain a pale-yellow oil. (2.68 g, Yield = 72%) ^{1}H NMR (CDCl$_3$, 500 MHz): δ_H 0.88 (t, 6.5 Hz, 3H), 1.24-1.30 (m, 18H), 1.38 (t, 7.0 Hz, 3H), 1.80 (t, 7.0 Hz, 2H), 4.33 (q, 7.0 Hz, 2H), 4.47 (t, 7.5 Hz, 2H), 6.92 (d, 5.0 Hz, 1H),7.19 (s, 1H), 7.30 (d, 5.5 Hz, 1H). ^{13}C NMR (CDCl$_3$, 125 MHz); δ_C 14.25, 14.56, 22.83, 27.02, 29.47, 29.67, 29.70, 29.75, 29.77, 31.28, 31.73, 32.05, 47.74, 60.15, 109.31, 110.48, 121.90, 126.32, 128.99, 145.24, 161.65

Synthesis of ethyl 4-dodecyl-4*H*-furo[3,2-*b*]pyrrole-5-carboxylate

To a 100 mL three neck round bottomed flask, ethyl 4*H*-furo[3,2-*b*]pyrrole-5-carboxylate (0.50 g, 2.79 mmol), anhydrous potassium carbonate (1.54 g, 5.58 mmol), 18-crown-6 ether (catalytic amount) and dry DMF (20.0 mL) were added under nitrogen. Solution was stirred at 80 °C for 3 h before adding 1-bromododecane (2.08 g, 4.18 mmol) dropwise. Resulting solution was refluxed for 24 h and cooled to room temperature. deionized water (50 mL) was added and neutralized using 3 M HCl. The organic layer was extracted with ethyl acetate (3 × 20 mL). The organic layer was washed with brine, dried over anhydrous magnesium sulfate and concentrated. The crude was purified by column chromatography using gradient elution starting from hexane: ethyl acetate: triethylamine (98:1:1 v/v) to hexane: ethyl acetate: triethylamine (94:5:1 v/v) as the eluent to obtain a pale-yellow oil. (0.97 g, Yield = 51%) ^{1}H NMR (CDCl$_3$, 500 MHz): δ_H 0.88 (t, 6.5 Hz, 3H), 1.24-1.29 (m, 18H), 1.36 (t, 7.0 Hz, 3H), 1.79 (t, 7.0 Hz, 2H), 4.29 (q, 7.0 Hz, 2H), 4.38 (t, 7.0 Hz, 2H), 6.43 (dd, 0.5 Hz and 2.0 Hz, 1H), 6.80 (d, 0.5 Hz, 1H), 7.49(d, 2.0 Hz, 1H). ^{13}C NMR (CDCl$_3$, 125 MHz); δ_C 14.26, 14.61, 22.83, 26.97, 29.45, 29.48, 29.68, 29.71, 29.76, 29.78, 31.15, 32.06, 47.81, 59.99, 98.35, 98.59, 123.47, 133.0, 145.82, 148.37, 162.14

Ethyl 4-dodecyl-2-(4,4,5,5-tetramethyl-1,3,2-dioxaborolan-2-yl)-4*H*-thieno[3,2-*b*]pyrrole-5-carboxylate

To a 50 mL single neck round bottomed flask, 4,4'-di-*tert*-butyl-2,2'-dipyridyl (dtbpy) (46 mg, 0.17 mmol), Ir[(μ_2-OMe)(COD)]$_2$ (57 mg, 0.086 mmol) and pinacolborane (0.3 mL) were added under nitrogen. Dry hexane (5.0 mL) and ethyl 4-dodecyl-4*H*-thieno[3,2-*b*]pyrrole-5-carboxylate (0.50 g, 1.72 mmol) were added to the flask and stirred for 48 h at room temperature. Pure compound was obtained after performing a flash column using hexane: ethyl acetate (99:1 v/v) as the eluent. (0.83 g, Yield = 99%) ^{1}H NMR (CDCl$_3$, 500 MHz): δ_H 0.87 (t, 10 Hz, 3H), 1.24-1.30 (m, 18H), 1.36 (s, 12H), 1.78 (t, 7.5 Hz, 2H), 4.31 (q, 5.0 Hz, 2H), 4.46 (t, 5.0 Hz, 2H), 7.17 (s, 1H), 7.45 (s, 1H). ^{13}C NMR (CDCl$_3$, 125 MHz); δ_C 14.25, 14.52, 22.82, 24.91, 24.99, 27.03, 29.47, 29.49, 29.70, 29.74, 29.76, 31.34, 32.05, 47.76,

60.35, 75.16, 84.41, 108.99, 119.49, 127.98, 128.34, 146.44, 161.68

Ethyl 4-dodecyl-2-(4,4,5,5-tetramethyl-1,3,2-dioxaborolan-2-yl)-4*H*-furo[3,2-*b*]pyrrole-5-carboxylate

To a 50 mL single neck round bottomed flask 4,4'-di-*tert*-butyl-2,2'-dipyridyl (dtbpy) (46 mg, 0.17 mmol), Ir[(μ_2-OMe)(COD)]$_2$ (57 mg, 0.086 mmol) and pinacolborane (0.3 mL) were added under nitrogen. Dry hexane (5.0 mL) and ethyl 4-dodecyl-4*H*-furo[3,2-*b*]pyrrole-5-carboxylate (0.50 g, 1.44 mmol) were added to the flask and stirred for 48 h at room temperature. The crude was purified by passing through a celite pad with hexane: ethyl acetate (8:2 v/v) solvent system to afford the pure compound. (0.51 g, 75%) ^{1}H NMR (CDCl$_3$, 500 MHz): δ_H 0.88 (t, 6.5 Hz, 3H), 1.23-1.30 (m, 18H), 1.37 (s, 12H), 1.77 (t, 10.0 Hz, 2H), 4.30 (q, 10.0 Hz, 2H), 4.37 (t, 5.0 Hz, 2H), 6.74 (s, 1H), 7.04 (s, 1H). ^{13}C NMR (CDCl$_3$, 125 MHz); δ_C 14.26, 14.58, 22.83, 24.92, 26.99, 29.46, 29.48, 29.67, 29.71, 29.76, 29.77, 31.09, 31.74, 32.06, 47.82, 60.22, 84.64, 97.99, 109.98, 126.36, 133.47, 150.09, 162.09

Synthesis of TP-FBT2T-TP

To a 100 mL three neck round bottomed flask, ethyl 4-dodecyl-2-(4,4,5,5-tetramethyl-1,3,2-dioxaborolan-2-yl)4*H*-thieno[3,2-*b*]pyrrole-5-carboxylate (0.83 g, 1.70 mmol), 4,7-bis(5-bromothiophen-2-yl)-5,6-difluorobenzo[*c*][1,2,5]thiadiazole (0.33 g, 0.68 mmol) and Pd(PPh$_3$)$_4$ (196 mg, 0.17 mmol) were added under nitrogen with anhydrous THF (25.0 mL). To the solution was added 2 M sodium carbonate (4.7 mL) and refluxed under nitrogen for 24 h. The flask was cooled to room temperature and crashed into cold methanol and resulted solid was filtered. Pure compound was obtained by column chromatography using hexane: methylene chloride 3:1 v/v as the eluent. (377.8 mg, Yield = 20%) ^{1}H NMR (CDCl$_3$, 500 MHz): δ_H 0.86 (t, 7.5 Hz, 3H), 1.25 (br, 18H), 1.38 (t, 5.0 Hz, 3H), 1.82 (t, 7.5 Hz, 2H), 4.31 (q, 5.0 Hz, 2H), 4.46 (t, 7.5 Hz, 2H), 7.12 (s, 1H), 7.13 (s, 1H), 7.29 (d, 5.0 Hz, 1H), 8.18 (d, 5.0 Hz, 1H). ^{13}C NMR (CDCl$_3$, 125 MHz); δ_C 14.25, 14.57, 22.83, 27.06, 29.49, 29.53, 29.74, 29.76, 29.78, 29.81, 31.34, 32.06, 47.81, 60.31, 107.32, 109.45, 121.74, 124.25, 126.59, 130.93, 132.01, 139.59, 141.83, 145.06, 148.79, 161.29 MALDI-TOF MS = 1058.1 g mol^{-1}, Theoretical mass = 1058.4 g mol^{-1}

Synthesis of FP-FBT2T-FP

Prepared using the same procedure as for **TP-FBT2T-TP** with ethyl 4-dodecyl-2-(4,4,5,5-tetramethyl-1,3,2-dioxaborolan-2-yl)-4*H*-furo[3,2-*b*]pyrrole-5-carboxylate and 1,4-dioxane as the solvent and potassium carbonate as the base. Pure compound was obtained by column chromatography using hexane: methylene chloride 2:3 v/v with 1% triethylamine as the eluent. (250.0 mg, Yield = 40%) ^{1}H NMR (CDCl$_3$, 500 MHz): δ_H 0.87 (t, 7.5 Hz, 3H), 1.25 (br, 18H), 1.38 (t, 7.5 Hz, 3H), 1.83 (t, 7.5 Hz, 2H), 4.31 (q, 5.0 Hz, 2H), 4.40 (t, 7.5 Hz, 2H), 6.70 (s, 1H), 6.80 (s, 1H), 7.45 (d, 5.0 Hz, 1H), 8.26 (d, 5.0 Hz, 1H). ^{13}C NMR (CDCl$_3$, 125 MHz); δ_C 14.27, 14.62, 22.84, 27.04, 29.50, 29.74, 29.76, 29.79, 29.81, 31.14, 32.07, 47.88, 58.07, 60.13, 94.23, 98.16, 111.46, 123.52, 124.11, 131.20, 131.85, 134.36, 137.11, 145.95, 148.69, 154.26, 161.80 MALDI-TOF MS = 1025.9 g mol^{-1}, Theoretical mass = 1026.4 g mol^{-1}
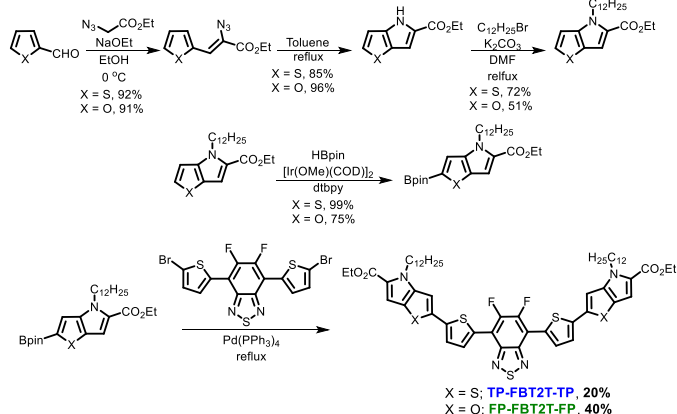
Scheme 1 Synthesis of **TP-FBT2T-TP** and **FP-FBT2T-FP**

Fig 2 DFT calculations performed on TP-FBT2T-TP' and FP-FBT2T-FP'

Results and Discussion

Material synthesis and characterization

The donor-acceptor molecules were synthesized according to Scheme 1. Commercially available 2-thiophenecarboxyaldehyde and furfural were first subjected to an aldol condensation reaction with a sacrificial electrophile (ethyl trifluoroacetate). The resulting acrylates were then cyclized by Hemetsberger cyclization. To impart solubility for the overall compounds, N-alkylation reactions were performed by deprotonation of pyrrolic hydrogen with potassium carbonate, and with subsequent addition of 1-bromododecane. Ethyl 4-dodecyl-4*H*-thieno[3,2-*b*]pyrrole-5-carboxylate was found to be stable in air, but ethyl 4-dodecyl-4*H*-furo[3,2-*b*]pyrrole-5-carboxylate was not stable in air for more than 1.5 h. Therefore, a borylation reaction was performed on the furo[3,2-*b*]pyrrole immediately after the column purification. However, after borylation the compound can be stored at cold temperatures for months without detecting any degradation. Borylation reactions were performed by using pinacolborane in the presence of Ir[(μ_2-OMe)(COD)]$_2$ catalyst to obtain borylated derivatives in high yields ($>$ 75%). Final Suzuki-Miyura coupling reactions were conducted in THF and 1,4-dioxane for **TP-FBT2T-TP** and **FP-FBT2T-FP**, respectively. Compounds were purified by column chromatography, and for the target small molecule comprising of furo[3,2-*b*]pyrrole, triethylamine (1%) was added to the eluent to stabilize the compound inside the column. Both small molecules were readily soluble in common organic solvents. However, furo[3,2-*b*]pyrrole containing small molecule was found to be more soluble. All the monomers and target organic semiconductors were fully characterized by ^{1}H and ^{13}C NMR spectroscopy and final organic semiconductors were additionally characterized by MALDI-TOF spectroscopy for mass evaluation (*see* Fig S21 and Fig S22).

Theoretical analysis

To investigate the frontier molecular orbital energy levels, density functional theory (DFT) calculations were performed
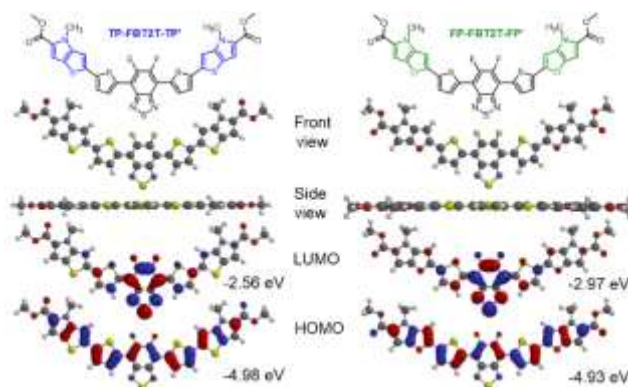
using Spartan'16 at B3LYP/6-31G* level of theory. *N*-Dodecane substituents and ethyl groups in the ester units were replaced by methyl groups to simplify the calculations as shown in Fig 2. Both molecules possess minimal torsion along the backbone to produce planar molecules. In our previous report, we have shown that substitution of smaller oxygen atom could lead to higher degree of backbone curvature due to the smaller carbon-oxygen bond distance.[46] When the substitution take place at the heteroacene unit, however, backbone curvature is unaffected. In terms of frontier orbital energy levels, the LUMO energy levels were somewhat different for the two small molecules although HOMO levels were comparable. **FP-FBT2T-FP** showed a relatively lower LUMO level suggesting insertion of furan units on to building blocks can effectively lower LUMO levels.

Optical and electrochemical analysis

To investigate absorption profiles of **TP-FBT2T-TP** and **FP-FBT2T-FP**, UV-vis spectroscopy was used in both solution and solid state (*see* Fig 3a). Interestingly, both small molecules showed two equally intense bands irrespective of the state (solution or solid state). Absorption bands present at lower wavelengths (higher energies) corresponds to π-π* transitions while bands at higher wavelengths (lower energies) are due to intramolecular charge transfer which takes place from HOMO to central 5,6-difluorobenzo[*c*][1,2,5]thiadiazole localized LUMO energy level. For **TP-FBT2T-TP** small molecule semiconductor, a small 10 nm bathochromic shift was observed for both absorption band maxima, suggesting the arrangement of molecules in solution and solid state are not very different.
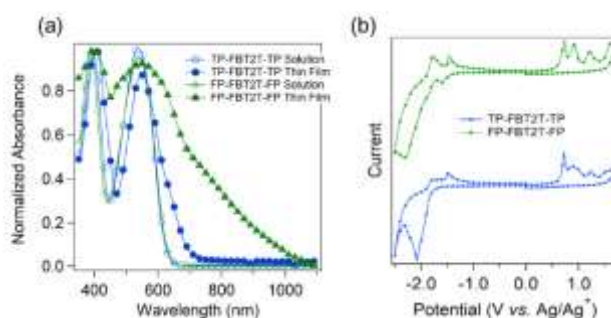

Fig 3 (a) UV-vis spectra of dilute chloroform solutions and drop-casted thin films, and (b) cyclic voltammetry spectra of **TP-FBT2T-TP** and **FP-FBT2T-FP** performed on thin films

ARTICLE

Journal Name

The onset of the absorption profile of **TP-FBT2T-TP** was estimated at 694 nm with an optical band gap of 1.79 eV. On the contrary, **FP-FBT2T-FP** semiconductor showed an extremely low optical band gap of 1.25 eV due to the extension of the absorption profile toward NIR II window in the solid state. Similar to **TP-FBT2T-TP**, 12-13 nm bathochromic shift was observed for the two absorption band maxima. Owing to the unstable nature of furan, **FP-FBT2T-FP** was stored in a nitrogen-filled glovebox for further characterization and tests.

To find the electrochemical band gaps and frontier molecular orbital energy levels, cyclic voltammetry measurements of thin films of the two small molecules were performed (*see* Fig 3b). Both small molecules showed multiple irreversible oxidation peaks, especially for **FP-FBT2T-FP** with more apparent and intensed peaks. Both small molecules showed two quasi-reversible reduction peaks in cyclic voltammograms as showed in Fig 3b. The HOMO and LUMO energy levels were estimated from the onset of the first oxidation and reduction peaks. For **TP-FBT2T-TP**, HOMO and LUMO levels were estimated at -5.07 eV and -2.60 eV, while for **FP-FBT2T-FP** it was -5.05 eV and -2.98 eV, respectively. These values were well matched with our DFT calculations performed with modelled compounds. Large mismatch between the optical and electrochemical band gaps could be due to exciton binding energies which could be 0.3 – 1.0 eV.[52] All optical and electrochemical properties are listed in Table 1.

OFET performances

The two donor-acceptor small molecules were tested in OFETs by employing a bottom-gate/ bottom-contact (BGBC) device architecture on Si/SiO$_2$ substrates. Both organic semiconductors, **TP-FBT2T-TP** and **FP-FBT2T-FP**, were dissolved in chloroform at 5 mg/mL and 10 mg/mL, respectively. Without any surface modification on SiO$_2$, no field-effect characteristics were shown irrespective of the annealing temperatures. Therefore, Si/SiO$_2$ surface was modified to obtain a self-

Table 1 Optical and electrochemical properties of **TP-FBT2T-TP** and **FP-FBT2T-FP**

Small molecule	[a]E_{HOMO}/ E_{LUMO} (eV)	[b]E_g^{ec}/ [c]E_g^{opt} (eV)	[d]λ_{max}^{sol} (nm)	[e]λ_{max}^{film} (nm)	[e]λ^{onset} (nm)
TP-FBT2T-TP	-5.07/ -2.60	2.47/ 1.79	384, 526	394, 537	694
FP-FBT2T-FP	-5.05/ -2.98	2.07/ 1.25	388, 537	400, 550	994

[a]Calculated from the onset of first oxidation and reduction peaks in cyclic voltammetry, [b]E_g^{ec} is calculated from -(E_{HOMO}-E_{LUMO}), [c]E_g^{opt} is calculated from 1242 nm / λ^{onset} , [d]calculated from the UV-vis spectra obtained in dilute chloroform solutions and [e]calculated from the UV-vis spectra obtained in thin-films

assembled monolayer (SAM) of octadecylsilane. After the application of the SAM, both small molecules were spun at 750 rpm inside a nitrogen filled glovebox and subsequently annealed at different temperatures inside the glovebox for 5 mins.

First, **TP-FBT2T-TP** small molecular semiconductor was analyzed in OFETs annealed at room temperature, 80 °C, 100 °C, 120 °C and 140 °C. As expected OFETs fabricated from **TP-FBT2T-TP** only showed p-type OFET characteristics. No apparent changes in hole mobilities, I_{on}/I_{off}, and V_T were observed when the annealing temperature was varied. All the thin films showed moderate hole mobility around 1.0×10^{-3} cm^2 /V s with I_{on}/I_{off} ratios ranging from 10^2 to 10^3. Threshold voltages were estimated to be around -3 V to -10 V depending on the annealing temperature. All the devices fabricated from **TP-FBT2T-TP** showed low leakage currents and clear saturation regimes. Subthreshold swings up to 0.7 V/dec were obtained for these devices. Most of all, the $I_D^{1/2}$ vs V_D curves did not display non-linearity that generally introduce errors when extracting mobilities from transfer curves.[53] All the transfer and output curves are shown in Fig 4. Summarized data for mobilities and OFET parameters can be found in Table 2.
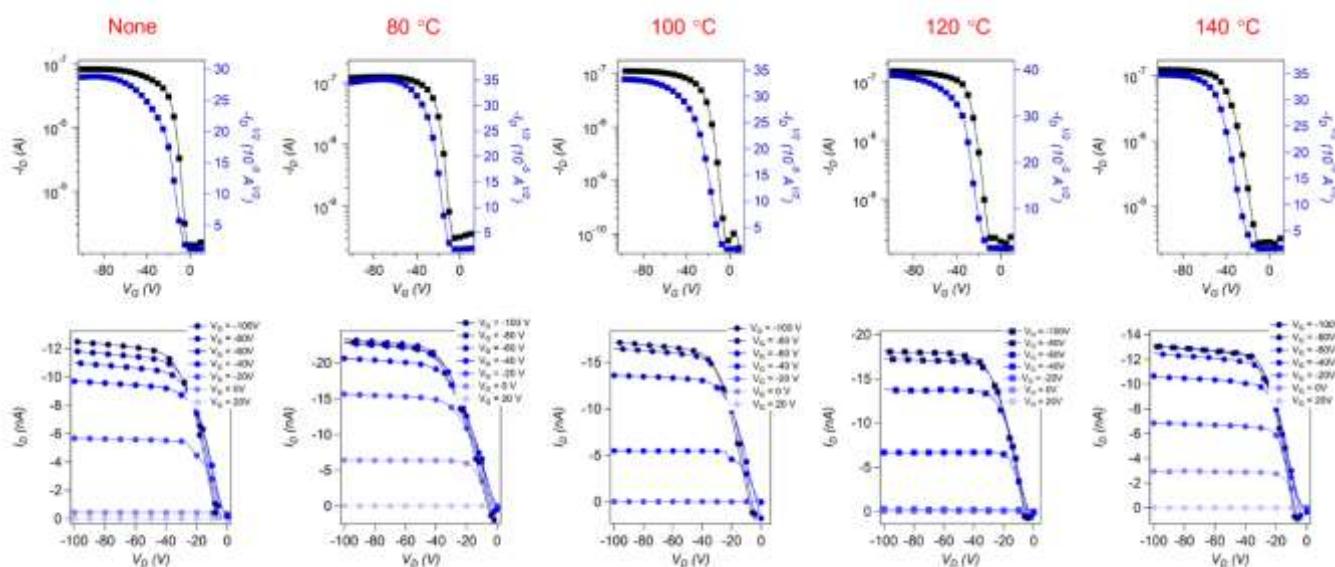

Fig 4 Transfer (top, V_D = -100 V) and output plots (bottom) of **TP-FBT2T-TP** at different annealing temperatures in BGBC OFET devices; W, L = 475, 20 μm

Table 2 Summary of OFET device performance **TP-FBT2T-TP** at different annealing conditions*

Annealing temperature	μ_{max}/μ_{ave} 10^{-3} cm^2/ V s	V_T (V)	I_{on}/I_{off}
None	0.93/ 0.81	-2.9 to -3.6	~10^2
80 °C	1.35/ 1.29	-5.7 to -2.4	~10^2
100 °C	0.97/ 0.82	-3.7 to -1.9	~10^3
120 °C	1.57/ 1.39	-9.6 to -4.9	~10^3
140 °C	0.71/ 0.58	-10.4 to -4.2	~10^2
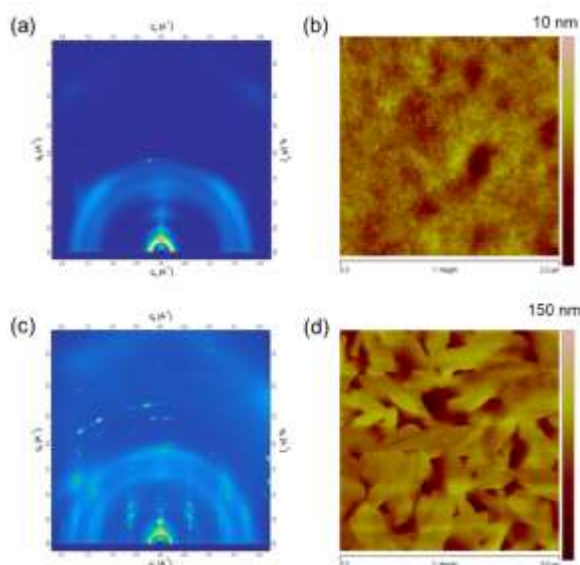
*average of six devices are shown in the table.

Fig 5 (a) GIWAXS spectrum, (b) TMAFM height image of **TP-FBT2T-TP** annealed at 120 °C, (c) GIWAXS spectrum and (d) TMAFM height image of **FP-FBT2T-FP** annealed at 100 °C

Surprisingly, **FP-FBT2T-FP** small molecule did not show any field-effect behaviour irrespective of the surface treatment, processing solvent and annealing temperature.

GIWAXS and TMAFM data

The complete OFET inactivity of **FP-FBT2T-FP** prompted us to investigate the GIWAXS patterns of the two small molecules. To probe the surface orientation with respect to the substrate, GIWAXS experiments were performed on thin films of **TP-FBT2T-TP** and **FP-FBT2T-FP** deposited on surface treated Si/SiO$_2$ substrates and are shown in Fig 5a and 5c, respectively. Scattering in the q$_z$ direction represents out-of-plane diffraction, and in the q$_y$ direction in-plane diffraction. Both small molecules (**TP-FBT2T-TP** and **FP-FBT2T-FP)** exhibit some degree of order, and although the crystal structure of these compounds is currently not available, we attribute the peaks near 0.25 Å^{-1} to stacking across the alkyl side chains. The effect of annealing on thin film microstructure along with out-of-plane and in-plane cuts are shown in Fig S23 and Fig S24.

Although significant scattering is apparent in the q$_z$ direction for **TP-FBT2T-TP**, the alkyl stacking peak shows significant scattering intensities away from the q$_z$ direction and the π-stacking feature at 1.8 Å^{-1} is nearly isotropic. Compared to **TP-FBT2T-TP**, **FP-FBT2T-FP** does not exhibit as much scattering in the q$_z$ direction, but many reflections are nevertheless apparent at various q$_y$ and q$_z$. For **FP-FBT2T-FP**, the multiple reflections away from the q$_y$ = 0 axis are similar to X-ray data for fluorinated benzothiadiazole acceptors, [54] and suggests strong texturing of the films.

Tapping mode atomic force microscopy (TMAFM) images were recorded in the channel region to probe surface morphology. Fig 5b shows the height image of **TP-FBT2T-TP** where no crystallized domains were present. On the other hand, **FP-FBT2T-FP** show large needle-like crystallites. A drastic change in the height (10 nm for **TP-FBT2T-TP** and 150 nm for **FP-FBT2T-FP**) was observed for thin films giving more texture which further explains the off-axis peaks in GIWAXS spectrum. Both height and phase images of the two small molecules are shown in Fig S25.

Conclusions

In the quest of searching for non-conventional building blocks for organic electronics, the smallest S,N-heteroacene and O,N-heteroacene were selected to study in OFETs. Donor-acceptor-donor type small molecules containing terminal thieno[3,2-*b*]pyrrole and furo[3,2-*b*]pyrrole with central 5,6-difluorobenzo[*c*][1,2,5]thiadiazole were successfully synthesized and characterized. Furo[3,2-*b*]pyrrole containing small molecule showed an enhanced absorption toward NIR I and NIR II regions. Both small molecules had similar HOMO levels, but furo[3,2-*b*]pyrrole containing molecule possessed a low lying LUMO level to realize a low band gap semiconductor. In terms of OFET performances, thieno[3,2-*b*]pyrrole containing small molecule was active, but furo[3,2-*b*]pyrrole containing small molecule was completely inactive.

Conflicts of interest

"There are no conflicts to declare".

Acknowledgements

Notes and references

1. A. Y. Amin, A. Khassanov, K. Reuter, T. Meyer-Friedrichsen and M. Halik, *J. Am. Chem. Soc.,* 2012, **134**, 16548-16550.
2. H. Minemawari, T. Yamada, H. Matsui, J. y. Tsutsumi, S. Haas, R. Chiba, R. Kumai and T. Hasegawa, *Nature*, 2011, **475**, 364.

3. J. Li, Y. Zhao, H. S. Tan, Y. Guo, C.-A. Di, G. Yu, Y. Liu, M. Lin, S. H. Lim, Y. Zhou, H. Su and B. S. Ong, *Sci. Rep.,* 2012, **2**, 754.

4. J. F. Martínez Hardigree and H. E. Katz, *Acc. Chem. Res.,* 2014, **47**, 1369-1377.

5. L. Xiang, W. Wang and W. Xie, *Sci. Rep.,* 2016, **6**, 36291.

6. M. Mas-Torrent and C. Rovira, *Chem. Rev.,* 2011, **111**, 4833-4856.

7. T. Izawa, E. Miyazaki and K. Takimiya, *Adv. Mater.*, 2008, **20**, 3388-3392.

8. H. K. H. Lee, Z. Li, I. Constantinou, F. So, S. W. Tsang and S. K. So, *Adv. Energy Mater.*, 2014, **4**, 1400768.

9. T. Vangerven, P. Verstappen, N. Patil, J. D'Haen, I. Cardinaletti, J. Benduhn, N. Van den Brande, M. Defour, V. Lemaur, D. Beljonne, R. Lazzaroni, B. Champagne, K. Vandewal, J. W. Andreasen, P. Adriaensens, D. W. Breiby, B. Van Mele, D. Vanderzande, W. Maes and J. Manca, *Chem. Mater.*, 2016, **28**, 9088-9098.

10. T. Vangerven, P. Verstappen, J. Drijkoningen, W. Dierckx, S. Himmelberger, A. Salleo, D. Vanderzande, W. Maes and J. V. Manca, *Chem. Mater.*, 2015, **27**, 3726-3732.

11. J. Du, C. Bulumulla, I. Mejia, G. T. McCandless, M. C. Biewer and M. C. Stefan, *Polym. Chem.*, 2017, **8**, 6181-6187.

12. H. Ebata, T. Izawa, E. Miyazaki, K. Takimiya, M. Ikeda, H. Kuwabara and T. Yui, *J. Am. Chem. Soc.,* 2007, **129**, 15732-15733.

13. G. Giri, E. Verploegen, S. C. B. Mannsfeld, S. Atahan-Evrenk, D. H. Kim, S. Y. Lee, H. A. Becerril, A. Aspuru-Guzik, M. F. Toney and Z. Bao, *Nature*, 2011, **480**, 504.

14. A. Dodabalapur, L. Torsi and H. E. Katz, *Science*, 1995, **268**, 270.

15. R. Hajlaoui, G. Horowitz, F. Garnier, A. Arce-Brouchet, L. Laigre, A. E. Kassmi, F. Demanze and F. Kouki, *Adv. Mater.*, 1997, **9**, 389-391.

16. Y. Sakamoto, T. Suzuki, M. Kobayashi, Y. Gao, Y. Fukai, Y. Inoue, F. Sato and S. Tokito, *J. Am. Chem. Soc.,* 2004, **126**, 8138-8140.

17. T. B. Singh, F. Meghdadi, S. Günes, N. Marjanovic, G. Horowitz, P. Lang, S. Bauer and N. S. Sariciftci, *Adv. Mater.*, 2005, **17**, 2315-2320.

18. S. Y. Yang, K. Shin and C. E. Park, *Adv. Funct. Mater.*, 2005, **15**, 1806-1814.

19. J. Li, K. Zhou, J. Liu, Y. Zhen, L. Liu, J. Zhang, H. Dong, X. Zhang, L. Jiang and W. Hu, *J. Am. Chem. Soc.,* 2017, **139**, 17261-17264.

20. C. He, A. Li, L. Yan, D. Zhang, Y. Zhu, H. Chen, H. Meng and O. Goto, *Adv. Electron. Mater.*, 2017, **3**, 1700282.

21. A. N. Lakshminarayana, A. Ong and C. Chi, *J. Mater. Chem. C*, 2018, **6**, 3551-3563.

22. A. N. Aleshin, J. Y. Lee, S. W. Chu, J. S. Kim and Y. W. Park, *Appl. Phys. Lett.*, 2004, **84**, 5383-5385.

23. C. Reese, W.-J. Chung, M.-m. Ling, M. Roberts and Z. Bao, *Appl. Phys. Lett.*, 2006, **89**, 202108.

24. O. D. Jurchescu, M. Popinciuc, B. J. van Wees and T. T. M. Palstra, *Adv. Mater.*, 2007, **19**, 688-692.

25. Y. Takeyama, S. Ono and Y. Matsumoto, *Appl. Phys. Lett.*, 2012, **101**, 083303.

26. R. Mondal, B. K. Shah and D. C. Neckers, *J. Am. Chem. Soc.,* 2006, **128**, 9612-9613.

27. M. Watanabe, Y. J. Chang, S.-W. Liu, T.-H. Chao, K. Goto, M. M. Islam, C.-H. Yuan, Y.-T. Tao, T. Shinmyozu and T. J. Chow, *Nat. Chem.*, 2012, **4**, 574.

28. S. S. Zade and M. Bendikov, *Angew. Chem. Int. Ed.*, 2010, **49**, 4012-4015.

29. C. Tönshoff and H. F. Bettinger, *Angew. Chem. Int. Ed.*, 2010, **49**, 4125-4128.

30. K. Xiao, Y. Liu, T. Qi, W. Zhang, F. Wang, J. Gao, W. Qiu, Y. Ma, G. Cui, S. Chen, X. Zhan, G. Yu, J. Qin, W. Hu and D. Zhu, *J. Am. Chem. Soc.,* 2005, **127**, 13281-13286.

31. Y. Liu, Y. Wang, W. Wu, Y. Liu, H. Xi, L. Wang, W. Qiu, K. Lu, C. Du and G. Yu, *Adv. Funct. Mater.*, 2009, **19**, 772-778.

32. X. Zhang, A. P. Côté and A. J. Matzger, *J. Am. Chem. Soc.,* 2005, **127**, 10502-10503.

33. T. Okamoto, K. Kudoh, A. Wakamiya and S. Yamaguchi, *Chem. Euro. J.*, 2007, **13**, 548-556.

34. J. Mei, Y. Diao, A. L. Appleton, L. Fang and Z. Bao, *J. Am. Chem. Soc.,* 2013, **135**, 6724-6746.

35. A. Dadvand, F. Cicoira, K. Y. Chernichenko, E. S. Balenkova, R. M. Osuna, F. Rosei, V. G. Nenajdenko and D. F. Perepichka, *Chem. Comm.*, 2008, 5354-5356.

36. M. Nakano, K. Niimi, E. Miyazaki, I. Osaka and K. Takimiya, *The J. Org. Chem.*, 2012, **77**, 8099-8111.

37. K. Takimiya, Y. Kunugi, Y. Konda, N. Niihara and T. Otsubo, *J. Am. Chem. Soc.,* 2004, **126**, 5084-5085.

38. I. Cho, S. K. Park, B. Kang, J. W. Chung, J. H. Kim, W. S. Yoon, K. Cho and S. Y. Park, *J. Mater. Chem. C*, 2016, **4**, 9460-9468.

39. J. Sim, K. Do, K. Song, A. Sharma, S. Biswas, G. D. Sharma and J. Ko, *Org. Electron.*, 2016, **30**, 122-130.

40. Y. Li, Y. Wu and B. S. Ong, *Macromolecules*, 2006, **39**, 6521-6527.

41. P.-L. T. Boudreault, S. Wakim, M. L. Tang, Y. Tao, Z. Bao and M. Leclerc, *J. Mater. Chem.*, 2009, **19**, 2921-2928.

42. C. Wetzel, E. Brier, A. Vogt, A. Mishra, E. Mena-Osteritz and P. Bäuerle, *Angew. Chem. Int. Ed.*, 2015, **54**, 12334-12338.

43. N. Arora, C. Wetzel, M. I. Dar, A. Mishra, P. Yadav, C. Steck, S. M. Zakeeruddin, P. Bäuerle and M. Grätzel, *ACS Appl. Mater. Interfaces*, 2017, **9**, 44423-44428.

44. J. Y. Shim, J. Baek, J. Kim, S. Y. Park, J. Kim, I. Kim, H. H. Chun, J. Y. Kim and H. Suh, *Polym. Chem.*, 2015, **6**, 6011-6020.

45. C. Jones, D. Boudinet, Y. Xia, M. Denti, A. Das, A. Facchetti and T. G. Driver, *Chem. Euro. J.*, 2014, **20**, 5938-5945.

46. C. Bulumulla, R. Gunawardhana, R. N. Kularatne, M. E. Hill, G. T. McCandless, M. C. Biewer and M. C. Stefan, *ACS Appl. Mater. Interfaces*, 2018, **10**, 11818-11825.

47. C. Bulumulla, R. N. Kularatne, R. Gunawardhana, H. Q. Nguyen, G. T. McCandless, M. C. Biewer and M. C. Stefan, *ACS Macro Lett.*, 2018, **7**, 629-634.

48. B. H. Smith, Q. Zhang, M. A. Kelly, J. H. Litofsky, D. Kumar, A. Hexemer, W. You and E. D. Gomez, *ACS Macro Lett.*, 2017, **6**, 1162-1167.

49. X. Wang, Z.-G. Zhang, H. Luo, S. Chen, S. Yu, H. Wang, X. Li, G. Yu and Y. Li, *Polym. Chem.*, 2014, **5**, 502-511.

50. H. Bronstein, J. M. Frost, A. Hadipour, Y. Kim, C. B. Nielsen, R. S. Ashraf, B. P. Rand, S. Watkins and I. McCulloch, *Chem. Mater.*, 2013, **25**, 277-285.

51. M. Wang, M. Ford, H. Phan, J. Coughlin, T.-Q. Nguyen and G. C. Bazan, *Chem. Comm.*, 2016, **52**, 3207-3210.

52. Y. Li, P. Singh Samarendra and P. Sonar, *Adv. Mater.*, 2010, **22**, 4862-4866.

53. H. Sirringhaus, *Adv. Mater.*, 2014, **26**, 1319-1335.

54. C. McDowell, K. Narayanaswamy, B. Yadagiri, T. Gayathri, M. Seifrid, R. Datt, S. Ryno, M. C. Heifner, V. Gupta, C. Risko, S. P. Singh and G. C. Bazan, *J. Mater. Chem. A*, 2018, **6**, 383-394.

TOC:
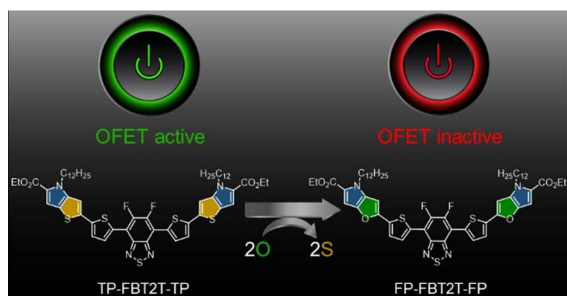
The smallest entries of S,N- and O,N-heteroacenes are systematically investigated in donor-acceptor-donor type small molecules toward OFETs.